Prospectivity model for magmatic Nickel, Copper, Cobalt, and Platinum-Group Elements in the Midcontinent Rift

Bezali K. Danso*
Independent Researcher, East Lansing, Michigan, USA
Email: dansobez@msu.edu
ORCID: 0009-0006-1201-4129

Adwoa A. Aidoo
Independent Researcher, Mine Geologist, Benso, Ghana
ORCID: 0009-0000-4363-8651

Saadatu Abdullah
Independent Researcher, Athens, Georgia, USA
ORCID: 0009-0003-9573-4479

*Corresponding author.

This manuscript is a **preprint** and has **not been peer reviewed**. It has been submitted to EarthArXiv. It has not yet been submitted to a journal for peer review. Subsequent versions of this manuscript may have slightly different content.

Data and code. Software and pipeline (riftprospect v0.1.1): doi:10.5281/zenodo.23697827; ranked target table and grid: doi:10.5281/zenodo.23697829; repository: `https://github.com/bkdanso/riftprospect`; interactive map: `https://bkdanso.github.io/riftprospect/`.

Prospectivity model for magmatic Nickel, Copper, Cobalt, and Platinum-Group Elements in the Midcontinent Rift

Bezali K. Danso [1,*] Adwoa A. Aidoo [2] and Saadatu Abdullah [3]

[1] *Independent Researcher, East Lansing, Michigan, USA*
[2] *Independent Researcher, Mine Geologist, Benso, Ghana*
[3] *Independent Researcher, Athens, Georgia, USA*

Much of the Midcontinent Rift is concealed beneath glacial sediment, which limits direct geological observation and makes it difficult to evaluate the potential for undiscovered magmatic Ni–Cu–PGE deposits with publicly available data. The 1.1 Ga rift hosts the Eagle Ni–Cu–PGE deposit of northern Michigan, one of the few domestic sources of nickel, a critical mineral of the United States. We address this problem with public geophysical and geochemical data from the Upper Peninsula of Michigan and northern Wisconsin. First, we develop a knowledge-driven prospectivity model from the new U.S. Geological Survey Earth MRI airborne magnetic and radiometric survey and apply it to 984,215 grid cells of 200 m (39,368.6 km^2). The model scores each cell by its similarity to the geophysical signature of a small mafic–ultramafic intrusion, propagates the uncertainty of the evidence weights by Monte Carlo simulation, and down-weights mapped iron formation and Keweenawan volcanic rocks. The Eagle deposit, withheld from model construction, ranks at the 98.9th percentile of the survey area (97.6th to 98.8th across 200 random weightings), so a search restricted to the highest-ranked 1.14% of the area would have included it. Second, we test whether public geochemical fertility indicators (Cu/Pd, Ni/Cu, MgO, and Mg-number) distinguish rocks near known Midcontinent Rift deposits from rocks farther away under spatially independent validation. Although Cu/Pd is lower near deposits (median 21,736 versus 31,568), predictive performance is poor: the area under the receiver operating characteristic curve (AUC) is 0.29 for a 3-km deposit buffer, and 0.48 and 0.35 for alternative buffers. We release 1,629 ranked exploration targets (751.8 km^2) with uncertainty estimates, an open-source Python workflow, and an interactive map. The results show that public airborne geophysical data can prioritize concealed critical-mineral targets, whereas currently available regional geochemical data provide only weak predictive discrimination.

Keywords: Midcontinent Rift, Eagle deposit, magmatic Ni–Cu–PGE sulfide, critical minerals, mineral prospectivity mapping, Earth MRI, aeromagnetics, airborne gamma-ray spectrometry, spatial cross-validation, open data

I. INTRODUCTION

Nickel, cobalt, copper, platinum, and palladium are designated critical minerals by the United States because of their importance to energy technologies, manufacturing, and national security [34]. Magmatic Ni–Cu–Co–PGE sulfide deposits are among the few deposit types that can supply all five commodities from a single ore system. They form when mantle-derived magmas become saturated in an immiscible sulfide liquid that concentrates the chalcophile metals [1, 2, 22]. The 1.1 Ga Midcontinent Rift (MCR) of the Lake Superior region hosts both the Duluth Complex Cu–Ni–PGE district of Minnesota [19] and the Eagle Ni–Cu–PGE deposit of Michigan [28], which demonstrates the fertility of rift-related mafic–ultramafic magmatism for critical-mineral mineralization.

Despite this endowment, discovering additional conduit-hosted Ni–Cu–PGE deposits remains difficult. Such deposits are small relative to deposits hosted by large, layered intrusions [14, 15], and much of the rift in Michigan and Wisconsin is concealed beneath glacial sediment. Geophysical and geochemical data are therefore increasingly used to identify prospective mafic–ultramafic intrusions and to prioritize areas for follow-up exploration, commonly within the framework of mineral prospectivity mapping, in which spatial evidence layers are combined according to a deposit model [4, 27].

The U.S. Geological Survey (USGS) Earth Mapping Resources Initiative (Earth MRI) was established to improve the geologic, geophysical, and geochemical framework needed to support domestic critical-mineral exploration [8]. In 2025, Earth MRI completed a high-resolution airborne magnetic and radiometric survey of Michigan's Upper Peninsula and northern Wisconsin [9]. Combined with the September 2026 release of the USGS Critical Mineral Deposits database [10] and the MCR-GeoChem geochemical compilation [5], these data provide an opportunity to evaluate whether publicly available information can identify concealed magmatic Ni–Cu–PGE systems in the rift.

The principal challenge is data scarcity. Within the 2025 survey area, the Eagle deposit is the only magmatic Ni–Cu–PGE deposit in the USGS database, which provides a single public deposit label; the other known MCR deposits of this type are in Minnesota, outside the survey footprint. Public geochemical coverage is sparse and uneven: although MCR-GeoChem contains 3,524

* dansobez@msu.edu

samples from Michigan, Minnesota, and Wisconsin, only 978 whole-rock samples lie within the survey area, none within 10 km of Eagle, and only 94 contain both Cu and Pd analyses. These limitations preclude conventional data-driven prospectivity methods, which rely on numerous known deposits and dense geochemical coverage [4].

We thus evaluate three questions using only publicly available data: (1) Can a knowledge-driven prospectivity model based solely on Earth MRI airborne magnetic and radiometric data recover a magmatic Ni–Cu–PGE deposit that was withheld from model construction? (2) Do public geochemical fertility indicators (Cu/Pd, Ni/Cu, MgO, and Mg-number) distinguish rocks near known magmatic Ni–Cu–PGE deposits from those farther away when evaluated with spatially independent cross-validation? (3) Can this data be used to generate a transparent, reproducible, and uncertainty-aware inventory of prospective exploration targets? To address these questions, we develop a rule-based geophysical prospectivity model, evaluate it against the Eagle deposit as a held-out test, assess the predictive value of public geochemical fertility indicators, and release a ranked inventory of exploration targets with quantified uncertainty, together with an open-source Python workflow [7] and an interactive map.

II. GEOLOGIC BACKGROUND AND DEPOSITS

The Midcontinent Rift is a Mesoproterozoic intracontinental rift system that formed at ca. 1.1 Ga and extends for more than 2,000 km beneath central North America, from Kansas through the Lake Superior region and southward beneath Michigan [3, 24]. Although rifting ultimately failed, and it has been proposed that the rift formed part of a larger plate-boundary system [32], it generated one of the largest episodes of continental mafic magmatism preserved on Earth, producing voluminous basaltic lava flows, mafic–ultramafic intrusions, dike and sill complexes, and thick syn-rift sedimentary sequences [24]. The exposed part of the rift around Lake Superior includes the Keweenawan volcanic succession, the Duluth Complex of northeastern Minnesota, the Beaver Bay Complex, the Mellen Intrusive Complex, numerous smaller mafic intrusions, and associated sedimentary basins [19, 24]. Geochemical and isotopic studies indicate contributions from multiple mantle sources and variable crustal contamination during rift evolution [23], and U–Pb geochronology shows that most magmatism occurred during a relatively brief interval near 1.1 Ga [25, 33].

The MCR hosts a spectrum of magmatic sulfide mineralization styles [28]. The largest known resources are in the Duluth Complex, where disseminated Cu–Ni–PGE mineralization is concentrated near the basal contacts of large intrusions [19]. In contrast, the Eagle deposit represents a conduit-style magmatic sulfide system hosted by a small mafic–ultramafic intrusion emplaced into Paleoproterozoic sedimentary rocks of the Baraga Basin [28]. Conduit-hosted deposits form where primitive magma is focused through narrow magma pathways, which promotes interaction with sulfur-bearing country rocks, sulfide saturation, and efficient concentration of Ni, Cu, Co, and the PGE [15, 22]. Although generally smaller than deposits in large layered intrusions, conduit systems can reach substantially higher grades and are important exploration targets in many large igneous provinces [2, 15].

In Michigan's Upper Peninsula, rift magmatism is represented by the Keweenawan volcanic succession of the Keweenaw Peninsula and the Porcupine Mountains, together with mafic and ultramafic intrusions emplaced into older Paleoproterozoic rocks. Many potential host intrusions are concealed beneath glacial sediment, which increases reliance on geophysical data. Mafic–ultramafic intrusions are attractive geophysical targets because they commonly contain abundant olivine, pyroxene, magnetite, and pyrrhotite, which make them denser and more magnetic than surrounding sedimentary and felsic crystalline rocks [22]. They also contain less potassium and thorium than adjacent granitoids and sedimentary rocks [20], so they produce distinctive magnetic and radiometric signatures.

Magnetic anomalies alone are not diagnostic of magmatic sulfide mineralization. The survey area also contains Paleoproterozoic banded iron formation of the Marquette, Gogebic, and Menominee iron ranges, and thick, magnetite-bearing Keweenawan basalt flows, all of which can produce strong magnetic responses unrelated to Ni–Cu–PGE mineralization. Large parts of the eastern survey area are covered by Paleozoic strata of the Michigan Basin, which conceal the Precambrian basement and increase geological uncertainty.

Geochemistry provides an additional line of evidence for magmatic sulfide fertility. Because palladium partitions far more strongly into sulfide liquid than copper, sulfide segregation preferentially removes Pd from silicate magma, so residual magmas develop elevated Cu/Pd ratios [2, 13]. Accordingly, low Cu/Pd may indicate sulfide accumulation, whereas anomalously high Cu/Pd commonly reflects prior sulfide depletion. Primitive magmas capable of carrying significant Ni and PGE are also generally characterized by high MgO, high Mg-number, and relatively high Ni/Cu [1, 22]. These relationships form the basis of widely used geochemical fertility indicators for mafic–ultramafic systems [13].

III. DATA

Table I summarizes the data. All were accessed on 27 October 2026; file provenance, access information, and SHA-256 checksums are recorded in a provenance log distributed with the code to ensure full reproducibility.

D1, USGS Critical Mineral Deposits of the United States. The USGS Critical Mineral Deposits database, version 3.0 (September 2026) [10], is a nationally standardized inventory of 1,271 critical-mineral deposits with

TABLE I. Data sources. PD: U.S. public domain.

ID	Source	Use in this study	Vintage	License	DOI
D1	USGS Critical Mineral Deposits of the United States [10]	Deposit labels; Eagle held-out test	ver. 3.0, Sept. 2026	CC0	10.5066/P9K1HBNT
D2	USGS airborne magnetic and radiometric survey, Upper Peninsula of Michigan and northern Wisconsin [9]	RTP, K, eTh, eU grids	flown 2025, released 2026	PD	10.5066/P14ESDF7
D3	MCR-GeoChem [5]	Cu/Pd, Ni/Cu, MgO, Mg-number per sample	v1.0.1, Oct. 2026	CC BY-SA 4.0	10.5281/zenodo.23516434
D4	USGS State Geologic Map Compilation [12]	Geology mask; cover flag	2017	PD	10.3133/ds1052
D5	USGS Mineral Resources Data System [35]	Secondary check only (not independent)	2011 snapshot	PD	–

deposit type, mineral-system classification, commodities, and coordinates. It serves here as the authoritative source of known magmatic Ni–Cu–PGE deposits and provides the labels for analysis and validation. In Michigan, Minnesota, and Wisconsin, 14 entries representing 11 deposits are classed as nickel–copper–PGE sulfide deposits of the mafic magmatic system: the Eagle mine in Michigan and, in Minnesota, nine Duluth Complex deposits (Birch Lake, Maturi, Maturi Southwest, Mesaba, NorthMet, Serpentine, Spruce Road, Wet Legs, and Wyman Creek) and the Tamarack deposit (four zones). All 14 entries are used to compute distances to known deposits. Within the 2025 survey area, Eagle is the only documented magmatic Ni–Cu–PGE deposit, which makes it the natural target for a held-out test. Because the database is a point inventory, its spatial precision is set by the reported coordinates rather than by a grid cell. It is released under CC0 and is the most current national compilation available, complementing global grade–tonnage inventories that underpin quantitative resource assessment [31].

D2, USGS airborne magnetic and radiometric survey. The Earth MRI survey of the Upper Peninsula of Michigan and northern Wisconsin [9] provides the primary geophysical evidence. It was flown between June and October 2025 at a nominal 100 m above terrain, with about 216,000 line-km in two blocks: Block A (west) on north–south lines 150 m apart with tie lines every 1,500 m, and Block B (east) on lines 400 m apart with tie lines every 4,000 m. We use the released grids of the reduced-to-pole (RTP) magnetic anomaly and of potassium (K, %), equivalent thorium (eTh, ppm), and equivalent uranium (eU, ppm), with cells of 37.5 m (Block A) and 100 m (Block B) in UTM zone 16N. The data are in the public domain and are well suited to identifying concealed mafic–ultramafic intrusions, because these bodies commonly combine elevated magnetic response with low K and Th, and because the survey provides consistent coverage where bedrock exposure is limited by glacial cover.

D3, MCR-GeoChem. MCR-GeoChem v1.0.1 [5] is a harmonized compilation of 3,524 Midcontinent Rift samples from Michigan, Minnesota, and Wisconsin drawn from six public sources, with consistent units, decoded below-detection values, best-value selection for each analyte, rift-membership labels, and quality flags. We use the whole-rock samples, their best values, and their alteration flag to calculate Cu/Pd, Ni/Cu, MgO, and Mg-number. Because it is focused on rift rocks and is the most comprehensive public geochemical compilation for the region, it is the most appropriate data set currently available for evaluating geochemical indicators of magmatic sulfide fertility. It is a sample-based compilation, so its spatial resolution depends on sample locations. It is licensed CC BY-SA 4.0.

D4, USGS State Geologic Map Compilation. The State Geologic Map Compilation (SGMC) [12] integrates state geologic mapping into a common national framework, with mapped units, generalized lithology, and age. We use its Michigan and Wisconsin polygons (1,148 features) to identify mapped lithologies, to distinguish areas underlain by sedimentary cover, and to construct the geology mask. Its spatial detail follows the mapped polygons. It is in the public domain.

D5, USGS Mineral Resources Data System. The Mineral Resources Data System (MRDS) [35] is a long-standing inventory of mineral occurrences, prospects, and mines whose record quality varies considerably. It is not used for training or validation. Its nickel-bearing records in Michigan and Wisconsin serve only as a secondary, qualitative check; because they informed one modeling decision (Sec. IV H), they are not an independent test.

IV. METHODS

A. Common grid

The two survey blocks were released with different acquisition parameters and grid resolutions. To create a uniform framework, every geophysical layer was resampled onto a common 200 m $\times$ 200 m grid in UTM zone

16N (EPSG:32616) by area-weighted averaging. This resolution preserves regional geophysical patterns while remaining comparable to the plan dimensions of small conduit-style intrusions such as Eagle. The final grid contains 984,215 cells (606,260 in Block A and 377,955 in Block B), covering 39,368.6 km^2.

Derivative layers were calculated from the RTP field T to highlight intrusive bodies. The three-dimensional analytic signal amplitude [21, 30],

$$|A| = \sqrt{\left(\frac{\partial T}{\partial x}\right)^2 + \left(\frac{\partial T}{\partial y}\right)^2 + \left(\frac{\partial T}{\partial z}\right)^2}, \qquad (1)$$

emphasizes the edges of magnetic sources regardless of magnetization direction; horizontal derivatives were computed by central differences and the vertical derivative by multiplying the Fourier transform of T by the wavenumber $|k|$. The residual field,

$$T_r = T - \overline{T}_{11\times 11}, \qquad (2)$$

is the RTP minus its mean over an 11×11-cell (2.2 km $\times$ 2.2 km) moving window and isolates local magnetic highs from regional trends. Because derivative products are susceptible to edge effects, the distance from each cell to the nearest cell without data was computed, and the 44,519 cells within 1 km of a data edge (4.5% of the grid) were excluded from target generation but retained for visualization.

B. Geophysical score

The model was designed to identify the geophysical signature of small mafic–ultramafic intrusions capable of hosting magmatic Ni–Cu–PGE mineralization: relatively magnetic, because they commonly contain magnetite and pyrrhotite, and low in K and Th relative to surrounding felsic and sedimentary rocks. Four evidence layers were selected on this basis (Table II).

Because the blocks were acquired with different line spacings, absolute values are not directly comparable across the survey. Each layer v was therefore converted to a percentile rank $p_v \in [0, 100]$ within its own block, and the percentile was transformed into a fuzzy membership value [27, 36] with a logistic function,

$$\mu_v = \left[1 + \exp\left(-\frac{\tilde{p}_v - m}{s}\right)\right]^{-1}, \qquad (3)$$

where $\tilde{p}_v = p_v$ for the magnetic layers, for which higher values are favorable, and $\tilde{p}_v = 100 - p_v$ for K and eTh, for which lower values are favorable; $m = 75$ is the midpoint and $s = 10$ the spread, in percentile units. The prospectivity score of a cell is the weighted mean of the memberships,

$$G = \frac{\sum_v w_v \, \mu_v}{\sum_v w_v}, \qquad (4)$$

TABLE II. Evidence layers of the geophysical score (Eq. 4).

Layer	Favorable	w_v
Analytic signal of RTP (Eq. 1)	high	0.35
Residual RTP (Eq. 2)	high	0.35
Potassium, K	low	0.15
Equivalent thorium, eTh	low	0.15

where a layer missing at a cell is omitted and the remaining weights are renormalized. Greater weight was assigned to the magnetic layers because magnetic fields reflect bedrock beneath glacial cover, whereas gamma rays originate in the uppermost few tens of centimeters and are attenuated by surficial sediment [20]. The analytic signal and the residual field were each assigned $w_v = 0.35$, and K and eTh each $w_v = 0.15$. All weights were defined from the deposit model before testing against Eagle.

C. Uncertainty

The weights and the membership midpoint are subjective, so their uncertainty was propagated by Monte Carlo simulation. In each of $N = 100$ realizations j, the weight vector was drawn from a Dirichlet distribution centered on the preferred weights $\mathbf{w}_0$,

$$\mathbf{w}^{(j)} \sim \mathrm{Dirichlet}(\kappa\, \mathbf{w}_0), \qquad m^{(j)} \sim \mathcal{U}(65, 85), \qquad (5)$$

with concentration $\kappa = 20$, and the midpoint was drawn uniformly between the 65th and 85th percentiles. The reported score of each cell is the mean over the realizations, $\bar{G} = N^{-1} \sum_j G^{(j)}$, and its uncertainty is the standard deviation σ_G.

D. Geology mask

Strong magnetic anomalies in the study area are not unique to mafic–ultramafic intrusions. Iron formation and magnetite-rich volcanic successions produce magnetic responses similar to those expected from prospective intrusions but are not generally associated with magmatic Ni–Cu–PGE mineralization. To reduce false positives, the score was multiplied by a class-dependent factor f_c from the SGMC (Table III),

$$S = f_c \, \bar{G}, \qquad \sigma_S = f_c \, \sigma_G. \qquad (6)$$

Mapped iron-formation units were buffered by 500 m, because their anomalies commonly extend beyond mapped contacts, and assigned $f_c = 0.3$. Mesoproterozoic volcanic units, including much of the Keweenawan lava succession, were assigned $f_c = 0.6$. Intrusive rocks and all other units retained $f_c = 1.0$. Areas beneath Phanerozoic sedimentary cover also retained $f_c = 1.0$ but were flagged, because magnetic sources beneath thick cover may be deep.

TABLE III. Geology mask classes from the SGMC, multipliers f_c (Eq. 6), and number of 200 m cells.

Class	f_c	Cells
Iron formation (+500 m)	0.3	33,120
Mesoproterozoic volcanic	0.6	54,037
Intrusive	1.0	25,182
Phanerozoic sedimentary cover	1.0	581,317
Other or unmapped	1.0	290,559

E. Geochemical fertility indicators and spatial cross-validation

Geochemical fertility indicators were used to evaluate whether public whole-rock geochemistry contains predictive information about magmatic Ni–Cu–PGE mineralization. For each MCR-GeoChem whole-rock sample,

$$\mathrm{Cu/Pd} = \frac{c_{\mathrm{Cu}}}{c_{\mathrm{Pd}}/1000}, \qquad \mathrm{Ni/Cu} = \frac{c_{\mathrm{Ni}}}{c_{\mathrm{Cu}}}, \tag{7}$$

with Cu and Ni in ppm and Pd in ppb, so that Cu/Pd is a ratio of concentrations in the same unit, and

$$\mathrm{Mg\#} = 100\,\frac{n_{\mathrm{Mg}}}{n_{\mathrm{Mg}} + 0.9\,n_{\mathrm{Fe^T}}}, \tag{8}$$

where n are molar abundances from MgO and total iron ($Fe_2O_3^T$), with Fe^{2+} taken as 90% of total iron. Ratios involving a below-detection value were treated as missing. Following the primitive-mantle Cu (30 ppm) and Pd (3.9 ppb) of McDonough and Sun [17], a reference Cu/Pd of 7,000 was adopted; samples with Cu/Pd $>$ 21,000 were classed as PGE-depleted, 2,333–21,000 as mantle-like, and $<$ 2,333 as PGE-enriched [2, 13].

Model development was restricted to Minnesota, which contains multiple known deposits and sufficient geochemical coverage. Only intrusive whole-rock samples not flagged as altered were used. Samples within 3 km of a known Ni–Cu–PGE deposit were labeled near ($y = 1$) and samples more than 10 km from all deposits far ($y = 0$); samples between 3 and 10 km were excluded to avoid ambiguous labels. The resulting data set comprises 467 samples (366 near, 101 far). A standardized logistic regression [26],

$$P(y = 1 \mid \mathbf{x}) = \left[1 + \exp\left(-\beta_0 - \boldsymbol{\beta}^{\top}\mathbf{z}\right)\right]^{-1}, \tag{9}$$

was fitted to the standardized features $\mathbf{z}$ of $\mathbf{x} = (\log_{10}\mathrm{Ni/Cu}, \mathrm{MgO}, \mathrm{Mg\#})$. Cu/Pd was excluded from the main model because Pd analyses are disproportionately concentrated near known deposits, so the presence or absence of a Pd measurement could itself reveal the label.

Performance was measured by the AUC [11], the probability that a randomly chosen near sample receives a higher predicted probability than a randomly chosen far sample (0.5 is chance), in five-fold grouped spatial cross-validation [29]. All near samples of a deposit, and all far samples within a 20 km block, were held out together, so performance reflects prediction of unseen deposits in unseen areas rather than interpolation between neighboring samples. The test was repeated with near radii of 2 and 5 km and with four alternative feature sets. Eagle could not contribute training data because no MCR-GeoChem sample lies within 10 km of it. Independently of any model, Cu/Pd of igneous samples near and far from deposits was compared with a two-sided Mann–Whitney test [16].

F. Targets and the held-out test

Targets were defined as connected groups (eight-neighbor) of cells whose final score S lies in the upper 2% of all non-edge cells ($S \geq 0.68$). No minimum size was imposed, because Eagle-style conduit intrusions may occupy only one cell at this resolution. Targets were ranked by peak score, with ties broken by area. For each target we recorded its center, area, peak and mean score, mean uncertainty, dominant mapped setting, distance to the nearest known Ni–Cu–PGE deposit, and, where available, the Cu/Pd class of the nearest igneous MCR-GeoChem sample within 5 km.

Eagle was excluded from all model development and weight selection. Because a deposit is recorded as a point, it was scored by the highest-scoring cell within 1 km of its coordinate (46.74815°N, 87.89729°W), S_E, and by its percentile among all n grid cells,

$$P_E = \frac{100}{n}\sum_{i=1}^{n}\mathbf{1}[S_i < S_E]\,. \tag{10}$$

The complement $100 - P_E$ is the percentage of the area that a search in descending order of scores would cover before reaching Eagle, and the probability that a randomly chosen location scores at least as high. The test was repeated with 200 further random weightings drawn as in Eq. 5, with equal weights, magnetic layers only, radiometric layers only, and without the geology mask.

G. Software

The workflow is a sequence of numbered Python scripts that download every input, log its provenance, build every output, and write every number quoted here to a statistics file from which this manuscript is generated. It uses pandas [18], scikit-learn [26], and standard scientific Python libraries. The reusable functions are released as the `riftprospect` package [7] with 14 unit tests.

H. Disclosures

Because the study relies on a single known deposit within the survey area, transparency about analyst decisions is essential. Several decisions were made after inspecting preliminary results. First, the raw percentile values at Eagle were examined during an early quality-control review of the grid, before the weights were finalized; weight selection was then based on the deposit model rather than on optimization against Eagle. Second, the minimum target size was originally three connected cells. Because Eagle's geophysical expression is a single-cell anomaly, it did not appear in the target list, and the criterion was removed; the original threshold would have produced 945 targets and excluded Eagle. Third, the geology mask was introduced after results highlighted the Pence iron mine and nickel occurrences on the Keweenaw Peninsula as highly ranked; these occurrences are therefore not independent validation data. Finally, five geochemical feature combinations and three near-deposit radii were evaluated. All results are reported, and none was selected preferentially. Every modeling decision, with its alternatives, is listed in Appendix B.

V. RESULTS

A. Survey, samples, and labels

Figure 1 shows the RTP field, the MCR-GeoChem samples, and the known deposits. The magnetic fabric of Block A records the Keweenawan lava pile of the Keweenaw Peninsula and the folded iron formations and intrusions of the Paleoproterozoic basins to the south, whereas the smoother field of Block B reflects the Paleozoic cover of the Michigan Basin. Of the 978 whole-rock samples inside the survey (920 in Michigan and 58 in Wisconsin), 664 are volcanic, 226 sedimentary, and only 63 intrusive; they cluster on the Keweenaw Peninsula and in the western Upper Peninsula.

B. Geophysical score and the held-out Eagle deposit

The geophysical score (Fig. 2A) highlights discrete clusters of high-scoring cells across the western and central survey, where strong magnetic signatures coincide with low K and Th, consistent with the expected expression of small mafic–ultramafic intrusions. The eastern block contains fewer anomalies: target density is 2.0 per 1,000 cells in Block A and 1.1 in Block B. The median score is 0.22. Uncertainty (Fig. 2B) is moderate: the median σ_G is 0.07 over the whole grid and 0.09 (about 12% of the score) among the top 2% of cells, and 99% of the cells in the top 2% under the preferred weights remain in the top 2% of the Monte Carlo mean. The ranking of the highest-scoring cells is therefore insensitive to plausible changes in weighting, even though individual scores vary.

TABLE IV. Percentile of the Eagle deposit (best cell within 1 km; Eq. 10) under alternative scoring schemes.

Variant	P_E
Final score (geology mask applied)	98.9
Geophysical score before mask	98.6
Equal weights (0.25 each)	98.1
Magnetic layers only	95.6
Radiometric layers only	88.4
200 random weightings, median	98.4
5th to 95th percentile	97.6 to 98.8

The model identifies the Eagle deposit although Eagle was excluded from model development. The Eagle cell is in the 90th percentile of Block A for analytic signal and the 94th for the residual field, and in the 23th and 17th for K and eTh, so it is low in both. Its final score, $S_E = 0.77 \pm 0.10$, places it at the 98.9th percentile after the geology mask (Table IV, Fig. 3A); a search guided by the map would examine only the highest-ranked 1.14% of the area before reaching Eagle.

The result is robust across model configurations. Before the mask, Eagle ranks at the 98.6th percentile, so its favorable score is driven by the geophysical evidence rather than by the geologic filter. Equal weights give the 98.1th percentile. Magnetic evidence alone places Eagle at the 95.6th percentile and radiometric evidence alone at the 88.4th, so magnetic data provide most of the discrimination and radiometric data a secondary refinement. Across 200 random weightings, Eagle's median percentile is 98.4, with a central 90% range of 97.6 to 98.8.

C. Secondary checks against MRDS

Four of the eight nickel-bearing MRDS records in Michigan and Wisconsin fall inside the survey. The Keweenaw "Michigan Nickel Deposits" records score at the 98.4th percentile before the mask and the 87.2th after it, because they lie on the masked lava succession. The past-producing Pence iron mine scores at the 98.8th percentile before the mask and still at the 98.0th after it, showing that the state-scale map does not capture every magnetic iron-formation body. The MRDS "Eagle Project" point, 3.2 km from the USGS deposit coordinate, scores at only the 48th percentile: for a target about one cell across, a location error of a few kilometers is enough to miss it. These records are not independent tests (Sec. IV H), but they illustrate the main source of false positives and the importance of accurate deposit coordinates.

D. Geochemical fertility indicators

In contrast to the geophysical results, the geochemical fertility indicators show little predictive ability under

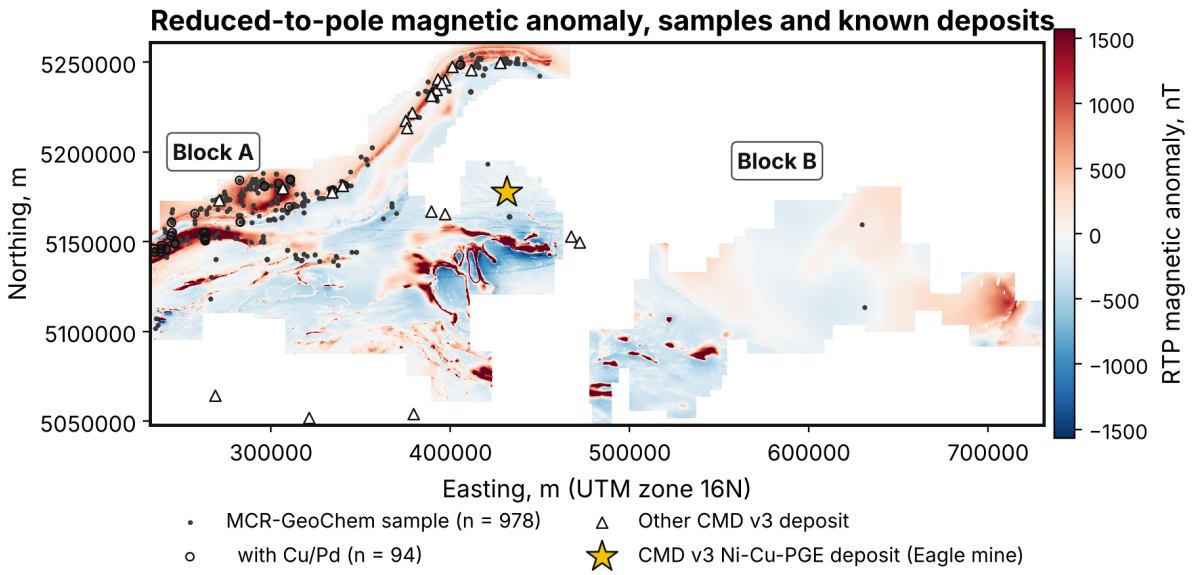

FIG. 1. The 2025 Earth MRI airborne survey [9]: reduced-to-pole magnetic anomaly on the 200 m grid, MCR-GeoChem whole-rock samples [5] (open circles: samples with Cu/Pd), USGS deposits [10] (triangles), and the Eagle deposit (star). UTM zone 16N.

spatial cross-validation. The main model (Ni/Cu, MgO, Mg-number) achieves an AUC of 0.29 (Table V, Fig. 3B), below the 0.5 expected for random discrimination. The result remains poor for other definitions of proximity: 0.48 for a 2 km and 0.35 for a 5 km near radius. An AUC well below 0.5 under grouped validation means that the relation learned on some deposits reverses on others, as expected when deposits differ in style and samples differ in origin.

Several alternative feature sets produced higher AUC values (Table V). Models with absolute Cu and Ni reached 0.65–0.66, and the model with Cu/Pd reached 0.74. These values should be interpreted cautiously. The Cu/Pd model rests on only 29 far samples, because Pd was analyzed mainly near deposits, so the availability of the data partly reveals the label; and the ranking of feature sets is unstable, the Cu, Ni, S model scoring 0.84 with a 2 km radius but 0.33 with 3 km. None of the feature sets was adopted.

Cu/Pd nevertheless differs with distance from deposits (Fig. 4). Igneous samples within 3 km of a deposit have a median Cu/Pd of 21,736 (n = 330), compared with 31,568 (n = 138) beyond 10 km (two-sided Mann–Whitney $p = 4.9\times10^{-7}$), and near-deposit samples extend to PGE-enriched values below 2,333, as expected for rocks containing accumulated sulfide [2]. However, many samples cluster around a few deposits, so the p-value overstates the amount of independent evidence. Lower Cu/Pd is consistent with sulfide fertility, but the signal is neither strong nor widespread enough to support regional prediction from public data alone.

TABLE V. Spatially cross-validated AUC of geochemical models (near: within 3 km of a deposit; far: beyond 10 km; Minnesota intrusive rocks). Main-model AUC for near radii of 2, 3, and 5 km: 0.48, 0.29, 0.35.

Features	AUC	n	near	far
Ni/Cu, MgO, Mg# (main)	0.29	467	366	101
Cu, Ni, MgO	0.65	600	490	110
Cu, Ni, MgO, Mg#, Cr, Co	0.66	446	365	81
Cu/Pd, Ni/Cu, MgO	0.74	270	241	29
Cu, Ni, S	0.33	318	283	35

E. Ranked targets

The geology-adjusted score produced 1,629 exploration targets with a combined area of 751.8 km^2, about 2% of the non-edge survey area (Fig. 5). Target sizes range from single-cell anomalies to clusters of up to 16.7 km^2; 459 targets consist of a single 200 m cell, consistent with the compact size expected for Eagle-style conduit intrusions, and the median area is 0.12 km^2.

Targets are unevenly distributed between survey blocks: Block A contains 1,233 and Block B 396. Most lie on units outside the masked classes (1,036) or beneath Phanerozoic sedimentary cover (507), and only 86 lie within mapped intrusive units. Much of the remaining

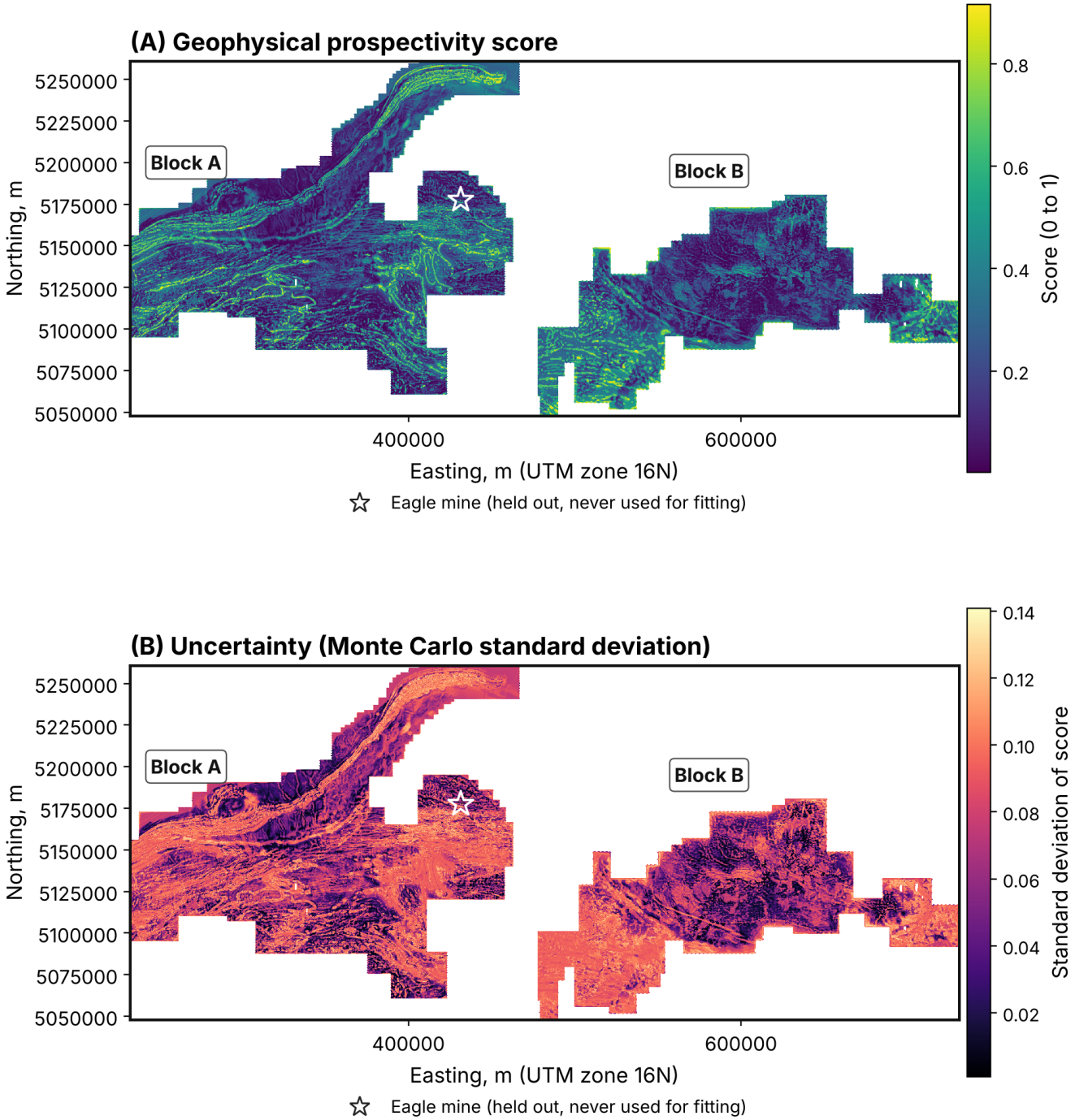

Score = weighted mean of analytic signal, residual magnetic field, low K and low eTh memberships (weights 0.35/0.35/0.15/0.15, decision D6).
Source: USGS 2025 airborne survey (doi:10.5066/P14ESDF7), 200 m cells, UTM zone 16N.

FIG. 2. (A) Geophysical score $\bar{G}$ (Eqs. 4 and 5), the mean of 100 Monte Carlo realizations, before the geology mask. (B) Its uncertainty σ_G. Star: the held-out Eagle deposit.

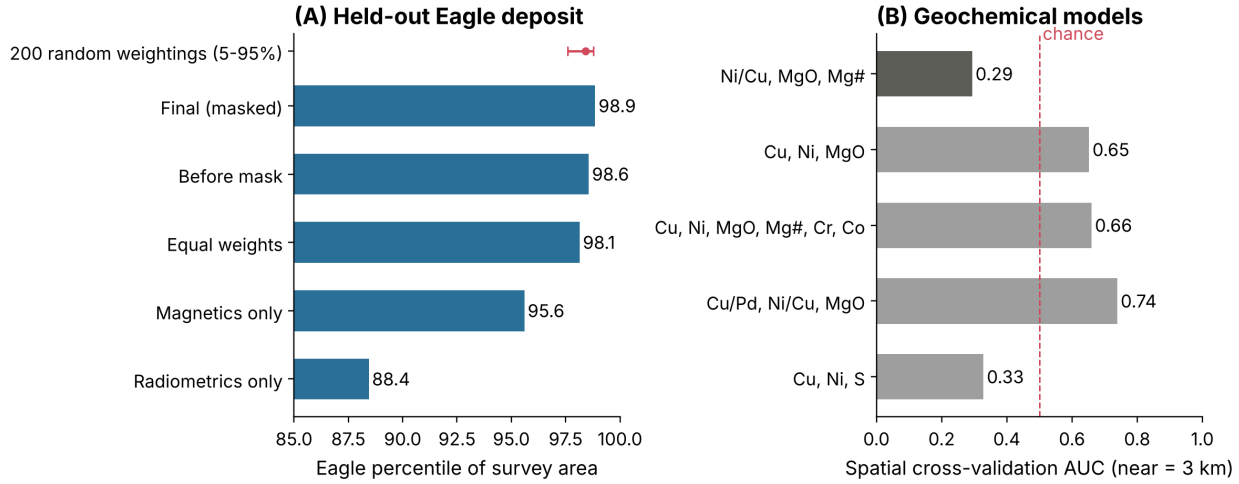

FIG. 3. (A) Percentile of the held-out Eagle deposit under each scoring variant; the red point and bar show the median and 5th–95th percentile range across 200 random weightings. (B) Spatially cross-validated AUC of the geochemical models; the dashed line marks chance.

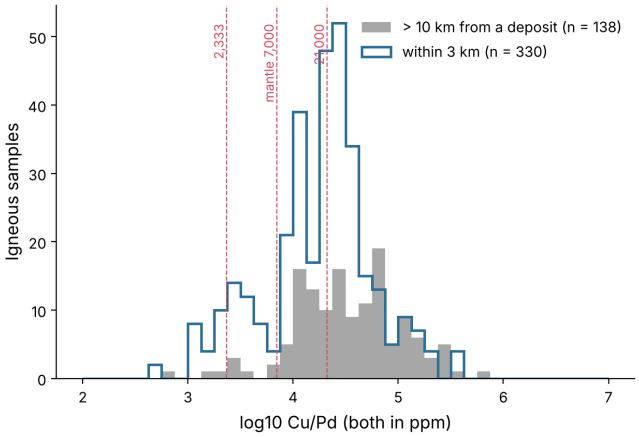

FIG. 4. Cu/Pd of igneous MCR-GeoChem samples within 3 km of a known Ni–Cu–PGE deposit (outline) and more than 10 km from all deposits (filled). Dashed lines: primitive-mantle reference [17] and class limits.

prospectivity therefore lies in areas with limited direct geological information rather than in previously recognized intrusions. Among the 50 highest-ranked targets, 39 are in Block A and 5 beneath cover; 20 targets lie within 10 km of Eagle and 112 within 25 km.

Geochemical information is available for few targets: only 45 of 1,629 have an igneous MCR-GeoChem sample within 5 km, so target prioritization rests almost entirely on geophysical evidence.

The Eagle anomaly is compact, and its peak score (0.77) is lower than the peak scores of many other targets, so the target containing Eagle ranks 724 of 1,629. Eagle is in the top 2% of the area but not near the top of the list. Membership in the target inventory is therefore more informative than small differences in rank within it.

TABLE VI. The ten highest-ranked targets. Setting: dominant SGMC class (Other: units outside the masked classes; Cover: Phanerozoic sedimentary cover).

Target	Lat.	Lon.	km^2	Peak	Setting
MCR-T0001	46.064	-90.358	1.84	0.911	Other
MCR-T0002	45.842	-88.027	1.08	0.908	Cover
MCR-T0003	46.528	-87.709	6.68	0.907	Other
MCR-T0004	45.930	-86.528	6.04	0.906	Cover
MCR-T0005	46.465	-87.807	6.04	0.906	Other
MCR-T0006	46.111	-86.716	2.88	0.905	Cover
MCR-T0007	46.525	-88.002	0.48	0.903	Other
MCR-T0008	46.287	-88.440	1.48	0.903	Other
MCR-T0009	46.376	-88.357	1.84	0.901	Other
MCR-T0010	45.783	-87.183	4.00	0.901	Cover

Table VI lists the ten highest-ranked targets. They represent the strongest combinations of magnetic and radiometric evidence after geologic filtering and are the most compelling candidates for field verification, ground geophysics, and, eventually, drilling.

VI. DISCUSSION

A. What the Eagle test demonstrates

The most important result is that a knowledge-driven model built entirely from public airborne geophysical data ranks the Eagle deposit among the most favorable locations in the 2025 survey area. Eagle was excluded from model construction and weight selection, yet the best cell within 1 km of the deposit ranks at the 98.9th percentile, so only 1.14% of the survey scores as high. The result is stable across equal weighting, magnetic-

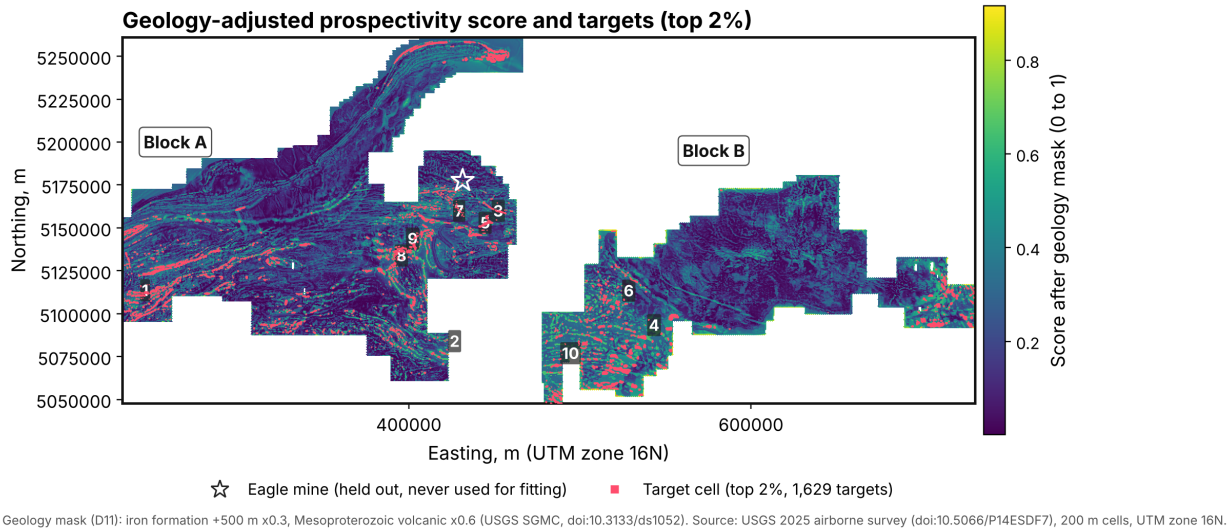

FIG. 5. Final prospectivity score S after the geology mask (Eq. 6), target cells (top 2% of non-edge cells, red), and the ten highest-ranked targets (labels). Star: the held-out Eagle deposit.

only scoring, and 200 random weightings, so it does not depend on a narrow set of parameter choices.

The held-out test indicates that the survey captures the geophysical characteristics expected of a conduit-hosted mafic–ultramafic intrusion. Eagle's response is driven mainly by the magnetic evidence, the analytic signal and the residual field, consistent with magnetite- and pyrrhotite-bearing ultramafic rocks [22, 28]. Radiometric data alone discriminate less well but improve performance in combination, so low K and Th provide useful complementary information.

The significance of this result should not be overstated. With only one known deposit in the study area, rigorous statistical validation is impossible. Ranking Eagle highly demonstrates consistency between the model and the deposit model, but it is not a calibrated measure of discovery success: a randomly chosen location would score as high 1.14% of the time. The decisions disclosed in Sec. IV H, including the change to the minimum target size and the introduction of the geology mask, also mean that the validation is not perfectly blind. The appropriate conclusion is limited but important: public airborne geophysical data contain enough information to identify a known Eagle-type system, and the resulting inventory is a transparent hypothesis that can be tested against future discoveries.

B. Why public geochemistry contributed little predictive power

The geochemical component yielded a very different outcome. The main fertility model performed at or below random expectation under spatially independent validation. This is initially surprising, because these indicators are widely used in magmatic sulfide exploration [2, 13], but three characteristics of the public data explain it.

First, the samples are not where the exploration problem is. Most MCR-GeoChem samples in the Upper Peninsula come from exposed Keweenawan volcanic rocks, whereas the principal exploration interest lies in concealed mafic–ultramafic intrusions in and around the Baraga Basin, and no public sample lies within 10 km of Eagle. The geochemical data therefore provide little direct information about the setting the model is trying to identify.

Second, all positive training samples come from Minnesota, mostly from the mineralized basal zones of the Duluth Complex [19]. The model consequently learns what distinguishes mineralized from unmineralized parts of the Duluth Complex rather than what characterizes magmatic sulfide systems across the rift, and relations that hold within one intrusive complex need not transfer to geologically distinct conduit-hosted systems such as Eagle [28].

Third, analytical coverage is biased by exploration history. Pd, S, and other fertility-related elements were preferentially analyzed in drill core from programs targeting known deposits, so models using them partly capture where exploration has occurred rather than where mineralization is favorable. This explains the apparently stronger, but unstable, performance of some alternative feature sets.

The lower Cu/Pd of near-deposit samples is nevertheless consistent with established models of sulfide saturation and PGE depletion [2, 13]. It appears to be driven largely by sampling around the Duluth Complex deposits rather than to represent an indicator that can be applied confidently across the survey area. The limitation is therefore not the indicators but the spatial distribution and analytical completeness of the public data. Addi-

tional modeling is unlikely to help until new data are collected: systematic sampling of mafic–ultramafic intrusions in the Baraga Basin and surrounding regions, with PGE analyses, would contribute more to regional assessment than further refinement of existing compilations.

C. False positives, geological complexity, and concealed targets

Not all magnetic anomalies represent ore-bearing intrusions. The Paleoproterozoic iron formations of the Marquette, Menominee, and Gogebic ranges produce strong anomalies that can resemble prospective intrusions, and thick Keweenawan basalt flows contain magnetite-rich units that raise magnetic response over large areas. The geology mask reduced these effects, but the continued high ranking of the Pence iron mine shows that regional mapping alone does not remove every non-prospective magnetic source. Future versions could improve discrimination with gravity data, more detailed lithologic mapping, depth-to-source estimates, and information extracted directly from the airborne line data.

Concealed terrain presents an additional challenge. 507 targets lie beneath Phanerozoic cover, where the depth to the magnetic source may vary considerably: some may represent shallow intrusions beneath thin cover and others deeply buried basement features of limited exploration value. Depth estimation would allow concealed targets to be ranked by probable drillability as well as by geophysical similarity.

D. Implications for exploration and future surveys

The target inventory is a screening tool, not a prediction of undiscovered deposits. It reduces a survey area of nearly 39,000 km^2 to about 750 km^2 of prioritized targets while preserving the uncertainty and geological context of each target, which makes reconnaissance-scale exploration considerably more efficient. The strongest targets combine favorable magnetic and radiometric characteristics while avoiding mapped iron formation and volcanic rocks; several lie beneath sedimentary cover, where conventional mapping provides little guidance, which highlights the value of airborne geophysics in covered terranes.

For geological surveys, the list provides a transparent framework for planning ground geophysics, mapping, geochemical sampling, and re-evaluation of drill core. For industry, it offers a reproducible set of areas that can be assessed with proprietary data. Because all inputs and methods are public, the results can also serve as a benchmark against which future prospectivity methods are evaluated.

E. Usage considerations

Scores are percentile-based and represent relative favorability rather than probability of mineralization; they rank locations within the survey and do not estimate resources or economic potential. Because percentiles were computed separately within the two blocks, small differences between Blocks A and B may reflect survey design rather than geology, so membership in the inventory is more informative than small differences in rank. Uncertainty is integral to the results: targets with similar scores but different uncertainties are not equally compelling. The score measures similarity to an Eagle-style deposit model and does not consider land access, permitting, resource size, economics, or metallurgy, and the Cu/Pd labels attached to a few targets are descriptive rather than predictive.

VII. LIMITATIONS

(1) Only one known magmatic Ni–Cu–PGE deposit, Eagle, lies within the survey, so predictive accuracy, discovery rates, and false-negative rates cannot be estimated with meaningful confidence. (2) The Eagle test is not perfectly blind (Sec. IV H); although the decisions are documented, some analyst bias cannot be excluded. (3) The final map is driven almost entirely by geophysics; the geochemical indicators failed spatial cross-validation and contribute only a descriptive attribute. (4) Unmapped or poorly mapped magnetic lithologies remain a significant source of false positives. (5) Depth to source is not estimated, so the 507 targets beneath sedimentary cover cannot be distinguished from shallow anomalies, and some may be too deep to be practical. (6) Block A was flown on 150 m and Block B on 400 m line spacing, so small intrusions are better resolved in the west. (7) Cells within 1 km of data edges, 4.5% of the area, were excluded from target generation. (8) Public geochemical coverage is sparse and spatially clustered: no sample lies within 10 km of Eagle, only 94 samples in the survey have both Cu and Pd, and statistical tests may overstate the independent evidence. (9) Absence from the USGS database does not imply absence of mineralization; undiscovered deposits, undocumented occurrences, and proprietary drilling, geophysical, and geochemical data are not represented. (10) The ten Minnesota deposits lie outside the survey footprint, so the geophysical method could not be tested against multiple deposits. Together, these limitations mean that the inventory should be viewed as a transparent, reproducible screening tool rather than a definitive prediction, to be re-evaluated as new discoveries, geophysical data, systematic geochemical sampling, and drilling become available.

VIII. CONCLUSIONS

A transparent, knowledge-driven prospectivity model based entirely on public data identifies geophysically favorable targets for magmatic Ni–Cu–PGE mineralization in the Midcontinent Rift. Using the 2025 Earth MRI airborne magnetic and radiometric survey, the held-out Eagle deposit ranks at the 98.9th percentile of the study area and remains highly ranked across a wide range of evidence weightings and model configurations, which indicates that the geophysical signature of an Eagle-style conduit intrusion is detectable at regional scale.

In contrast, public geochemical fertility indicators showed limited predictive value under spatially independent validation. Although Cu/Pd is systematically lower near known deposits, models based on Ni/Cu, MgO, and Mg-number failed to discriminate deposit-proximal from distal samples once whole deposits and areas were withheld from training. The principal limitation is the uneven spatial distribution of samples and analyses rather than the indicators themselves.

These findings lead to two complementary conclusions. First, the Earth MRI survey contains enough geophysical information to identify Eagle-type targets and supports a reproducible inventory of 1,629 ranked targets across the Upper Peninsula of Michigan and northern Wisconsin. Second, improvements in regional prospectivity mapping are more likely to come from new geochemical data than from more sophisticated modeling of existing data; systematic whole-rock and PGE sampling of the Baraga Basin intrusions and other rift mafic–ultramafic bodies would substantially strengthen future assessments. We release the target inventory [6], uncertainty estimates, interactive map, and the `riftprospect` workflow [7]. Future versions will incorporate gravity data, depth-to-source estimates, higher-resolution geology, and occurrence records from the state geological surveys, so that the framework can be re-evaluated and improved as new discoveries and data become available.

DATA AND CODE AVAILABILITY

The `riftprospect` v0.1.1 software and workflow are archived at doi:10.5281/zenodo.23697827 (MIT license) [7], installable with `pip install riftprospect`, and developed at `https://github.com/bkdanso/riftprospect`. The ranked target table, the 200 m grid with every evidence layer and score, and the validation statistics are archived at doi:10.5281/zenodo.23697829 (CC BY-SA 4.0) [6]. The interactive map is at `https://bkdanso.github.io/riftprospect/`. Every number in this paper is generated from the statistics files in the repository. Users should also cite the original data sources [5, 9, 10, 12, 35].

AUTHOR CONTRIBUTIONS

Bezali K. Danso: conceptualization, methodology, formal analysis, validation, data curation, writing (original draft), and project administration. Adwoa A. Aidoo: validation (verification and review of the known deposits used for training and testing, the held-out Eagle location, and the MRDS occurrences used as secondary checks) and writing (review and editing). Saadatu Abdullah: formal analysis, review, and visualization (the airborne geophysics component of the map: magnetic and radiometric evidence layers, the geology mask, and review of the score, uncertainty, and target maps) and writing (review and editing). All authors approved the final manuscript.

USE OF AI TOOLS

AI tools (Claude, Anthropic; GitHub Copilot; ChatGPT, OpenAI) were used to assist with code development, testing, debugging, and editing during this study. The authors made all methodological and modeling decisions, verified all data processing and analytical results, interpreted the findings, and prepared the manuscript text. AI tools were used solely as aids to improve efficiency and did not contribute independently to the study design, scientific conclusions, or final interpretations.

COMPETING INTERESTS AND FUNDING

The authors declare no competing interests. This research received no external funding.

ACKNOWLEDGMENTS

We thank the U.S. Geological Survey for the Earth MRI airborne survey, the Critical Mineral Deposits database, the State Geologic Map Compilation, and the Mineral Resources Data System, and the data authors whose analyses are compiled in MCR-GeoChem, for making their data openly available.

REFERENCES

[1] Nicholas T. Arndt, C. Michael Lesher, and Gerald K. Czamanske. Mantle-derived magmas and magmatic Ni–Cu–(PGE) deposits. In *Economic Geology 100th Anniversary Volume*, pages 5–24. Society of Economic Geologists, 2005.

[2] Sarah-Jane Barnes and Peter C. Lightfoot. Formation of magmatic nickel sulfide ore deposits and processes affecting their copper and platinum group element contents. In *Economic Geology 100th Anniversary Volume*, pages 179–213. Society of Economic Geologists, 2005.

[3] W. F. Cannon, A. G. Green, D. R. Hutchinson, *et al.* The North American Midcontinent Rift beneath Lake Superior from GLIMPCE seismic reflection profiling. *Tectonics*, 8(2):305–332, 1989. doi:10.1029/TC008i002p00305

[4] Emmanuel John M. Carranza. *Geochemical Anomaly and Mineral Prospectivity Mapping in GIS*. Handbook of Exploration and Environmental Geochemistry, vol. 11. Elsevier, Amsterdam, 2008.

[5] Bezali K. Danso and Saadatu Abdullah. MCR-GeoChem v1.0.1: harmonized whole-rock and mineral geochemistry of the Midcontinent Rift (Michigan, Minnesota, Wisconsin). Zenodo, 2026. doi:10.5281/zenodo.23516434

[6] Bezali K. Danso, Adwoa A. Aidoo, and Saadatu Abdullah. Ranked prospectivity targets for magmatic Ni-Cu-Co-PGE deposits, Upper Peninsula of Michigan and northern Wisconsin (v0.1.0). Zenodo, 2026. doi:10.5281/zenodo.23697829

[7] Bezali K. Danso, Adwoa A. Aidoo, and Saadatu Abdullah. riftprospect v0.1.1: open prospectivity model for magmatic Ni-Cu-Co-PGE deposits in the Midcontinent Rift. Zenodo, 2026. doi:10.5281/zenodo.23697827

[8] Warren C. Day. The Earth Mapping Resources Initiative (Earth MRI): Mapping the Nation's critical mineral resources. U.S. Geological Survey Fact Sheet 2019–3007, 2019. doi:10.3133/fs20193007

[9] Benjamin J. Drenth, Joshua T. Murchek, Philip J. Brown II, and Daniel M. Connell. Airborne magnetic and radiometric survey, Upper Peninsula, Michigan, and parts of northern Wisconsin, 2025. U.S. Geological Survey data release, 2026. doi:10.5066/P14ESDF7

[10] Jane M. Hammarstrom, Laurel G. Woodruff, Connie L. Dicken, and Terri A. Zach. Critical mineral deposits of the United States (ver. 3.0, September 2026). U.S. Geological Survey data release, 2026. doi:10.5066/P9K1HBNT

[11] James A. Hanley and Barbara J. McNeil. The meaning and use of the area under a receiver operating characteristic (ROC) curve. *Radiology*, 143(1):29–36, 1982. doi:10.1148/radiology.143.1.7063747

[12] John D. Horton, Carma A. San Juan, and Douglas B. Stoeser. The State Geologic Map Compilation (SGMC) geodatabase of the conterminous United States. U.S. Geological Survey Data Series 1052, 2017. doi:10.3133/ds1052

[13] Chusi Li, Wolfgang D. Maier, and Sarel A. de Waal. Magmatic Ni-Cu versus PGE deposits: Contrasting genetic controls and exploration implications. *S. Afr. J. Geol.*, 104(4):309–318, 2001. doi:10.2113/gssajg.104.4.309

[14] Peter C. Lightfoot. *Nickel Sulfide Ores and Impact Melts: Origin of the Sudbury Igneous Complex*. Elsevier, Amsterdam, 2017.

[15] Peter C. Lightfoot and Dawn Evans-Lamswood. Structural controls on the primary distribution of mafic–ultramafic intrusions containing Ni–Cu–Co–(PGE) sulfide mineralization in the roots of large igneous provinces. *Ore Geol. Rev.*, 64:354–386, 2015.

[16] H. B. Mann and D. R. Whitney. On a test of whether one of two random variables is stochastically larger than the other. *Ann. Math. Stat.*, 18(1):50–60, 1947. doi:10.1214/aoms/1177730491

[17] William F. McDonough and Shen-su Sun. The composition of the Earth. *Chem. Geol.*, 120(3–4):223–253, 1995.

[18] Wes McKinney. Data structures for statistical computing in Python. In *Proc. 9th Python in Science Conf.*, pages 56–61, 2010. doi:10.25080/Majora-92bf1922-00a

[19] James D. Miller Jr., John C. Green, Mark J. Severson, Val W. Chandler, Steven A. Hauck, Dean M. Peterson, and Terrence E. Wahl. Geology and mineral potential of the Duluth Complex and related rocks of northeastern Minnesota. Minnesota Geological Survey Report of Investigations 58, 207 p., 2002.

[20] Brian R. S. Minty. Fundamentals of airborne gamma-ray spectrometry. *AGSO J. Aust. Geol. Geophys.*, 17(2):39–50, 1997.

[21] Misac N. Nabighian. The analytic signal of two-dimensional magnetic bodies with polygonal cross-section: Its properties and use for automated anomaly interpretation. *Geophysics*, 37(3):507–517, 1972. doi:10.1190/1.1440276

[22] Anthony J. Naldrett. *Magmatic Sulfide Deposits: Geology, Geochemistry and Exploration*. Springer, Berlin, 2004.

[23] Suzanne W. Nicholson, Klaus J. Schulz, Steven B. Shirey, and John C. Green. Rift-wide correlation of 1.1 Ga Midcontinent rift system basalts: Implications for multiple mantle sources during rift development. *Can. J. Earth Sci.*, 34(4):504–520, 1997. doi:10.1139/e17-041

[24] Richard W. Ojakangas, G. B. Morey, and John C. Green. The Mesoproterozoic Midcontinent Rift System, Lake Superior Region, USA. *Sediment. Geol.*, 141–142:421–442, 2001. doi:10.1016/S0037-0738(01)00085-9

[25] James B. Paces and James D. Miller Jr. Precise U-Pb ages of Duluth Complex and related mafic intrusions, northeastern Minnesota: Geochronological insights to physical, petrogenetic, paleomagnetic, and tectonomagmatic processes associated with the 1.1 Ga Midcontinent Rift System. *J. Geophys. Res. Solid Earth*, 98(B8):13997–14013, 1993. doi:10.1029/93JB01159

[26] Fabian Pedregosa, Gaël Varoquaux, Alexandre Gramfort, *et al.* Scikit-learn: Machine learning in Python. *J. Mach. Learn. Res.*, 12:2825–2830, 2011.

[27] Alok Porwal, E. J. M. Carranza, and M. Hale. Knowledge-driven and data-driven fuzzy models for predictive mineral potential mapping. *Nat. Resour. Res.*, 12(1):1–25, 2003.

[28] Edward M. Ripley. Ni-Cu-PGE mineralization in the Partridge River, South Kawishiwi, and Eagle intrusions: A review of contrasting styles of sulfide-rich occurrences in the Midcontinent Rift System. *Econ. Geol.*, 109(2):309–324, 2014. doi:10.2113/econgeo.109.2.309

[29] David R. Roberts, Volker Bahn, Simone Ciuti, *et al.* Cross-validation strategies for data with temporal, spatial, hierarchical, or phylogenetic structure. *Ecography*, 40(8):913–929, 2017. doi:10.1111/ecog.02881

[30] Walter R. Roest, Jacob Verhoef, and Mark Pilkington. Magnetic interpretation using the 3-D analytic signal. *Geophysics*, 57(1):116–125, 1992. doi:10.1190/1.1443174

[31] Donald A. Singer, Vladimir I. Berger, and Barry C. Moring. Porphyry copper deposits of the world: Database and grade and tonnage models, 2008. U.S. Geological Survey

Open-File Report 2008-1155, 2008.

[32] Carol A. Stein, Seth Stein, Miguel Merino, G. Randy Keller, Lucy M. Flesch, and Donna M. Jurdy. Was the Midcontinent Rift part of a successful seafloor-spreading episode? *Geophys. Res. Lett.*, 41(5):1465–1470, 2014. doi:10.1002/2013GL059176

[33] Nicholas L. Swanson-Hysell, Steven A. Hoaglund, James L. Crowley, Mark D. Schmitz, Yiming Zhang, and James D. Miller Jr. Rapid emplacement of massive Duluth Complex intrusions within the North American Midcontinent Rift. *Geology*, 49(2):185–189, 2021. doi:10.1130/G47873.1

[34] U.S. Geological Survey. Interior Department releases final 2025 List of Critical Minerals. USGS Science Snippet, November 2025. `https://www.usgs.gov/news/science-snippet/interior-department-releases-final-2025-list-critical-minerals`

[35] U.S. Geological Survey. Mineral Resources Data System (MRDS). U.S. Geological Survey, Reston, Virginia. `https://mrdata.usgs.gov/mrds/` (accessed 2026-10-27).

[36] Mahyar Yousefi and Emmanuel John M. Carranza. Fuzzification of continuous-value spatial evidence for mineral prospectivity mapping. *Comput. Geosci.*, 74:97–109, 2015.

Appendix A: Target table columns

Table VII defines the columns of the released target table.

TABLE VII. Columns of the released target table (`targets_ranked.csv`).

Column	Meaning
target_id	Permanent identifier, MCR-T + rank
rank	1 = highest peak score
latitude, longitude	Target center, WGS84
area_km2	Number of cells $\times$ 0.04 km^2
score_mean, score_max	Mean and peak final score S
score_sd_mean	Mean Monte Carlo uncertainty σ_S
block	Survey block, A or B
geo_class	Dominant SGMC class
cu_pd_label	Cu/Pd class of nearest igneous sample within 5 km
km_to_known_ni_cu_pge	Distance to nearest USGS Ni–Cu–PGE deposit

Appendix B: Modeling decisions

Table VIII lists every modeling decision, its setting, and the main alternatives considered.

TABLE VIII. Modeling decisions, settings, and the main alternatives considered.

ID	Decision	Setting (alternatives)
D1	Label strategy	Geochemistry trained in Minnesota; geophysics knowledge-driven; Eagle held out (positive-unlabeled learning on 3–4 positives; rule-based only)
D2	Near radius	3 km near, >10 km far (2 or 5 km)
D3	Fe^{2+} share for Mg#	0.9 (0.85, 1.0)
D4	Below-detection values in ratios	Treated as missing (half the limit)
D5	Cu/Pd classes	Reference 7,000; $\times$3 and $\div$3
D6	Evidence weights	0.35/0.35/0.15/0.15; midpoint 75th percentile (equal weights)
D7	Targets	Top 2% of non-edge cells; single cells allowed (top 1%; minimum three cells)
D8	Geochemical training rocks	Intrusive, not flagged altered (all igneous)
D9	Role of geochemistry	Descriptive label only (geochemical score blended with weight 0.3)
D10	Reach of Cu/Pd label	5 km (2, 10 km)
D11	Geology mask	Iron formation +500 m $\times$0.3; Mesoproterozoic volcanic $\times$0.6 (no mask)
D12	Phanerozoic cover	Flagged, not down-weighted (down-weighted; excluded)
QA	Edge rule	Cells within 1 km of a data edge cannot be targets